Design of Functionalized Lipids and Evidence for Their Binding to Photosystem II Core Complex by Oxygen Evolution Measurements, Atomic Force Microscopy, and Scanning Near-Field Optical Microscopy

Eric Trudel,* Judith Gallant,* Stéphane Mons,† Charles Mioskowski,† Luc Lebeau,† Karin Jeuris,‡ Philippe Foubert,‡ Frans De Schryver,‡ and Christian Salesse*

*Département de Chimie-Biologie, Université du Québec à Trois-Rivières, Trois-Rivières, Québec G9A 5H7, Canada; †Laboratoire de Synthèse Bioorganique associé au CNRS, Faculté de Pharmacie, Université Louis Pasteur de Strasbourg, 67 401 Illkirch, France; and ‡Department of Chemistry, Katholieke Universiteit Leuven, 3001 Heverlee-Leuven, Belgium

ABSTRACT Photosystem II core complex (PSII CC) absorbs light energy and triggers a series of electron transfer reactions by oxidizing water while producing molecular oxygen. Synthetic lipids with different alkyl chains and spacer lengths bearing functionalized headgroups were specifically designed to bind the Q_B site and to anchor this large photosynthetic complex (240 kDa) in order to attempt two-dimensional crystallization. Among the series of different compounds that have been tested, oxygen evolution measurements have shown that dichlorophenyl urea (DCPU) binds very efficiently to the Q_B site of PSII CC, and therefore, that moiety has been linked covalently to the headgroup of synthetic lipids. The analysis of the monolayer behavior of these DCPU-lipids has allowed us to select ones bearing long spacers for the anchoring of PSII CC. Oxygen evolution measurements demonstrated that these long-spacer DCPU-lipids specifically bind to PSII CC and inhibit electron transfer. With the use of atomic force microscopy (AFM) and scanning near-field optical microscopy (SNOM), it was possible to visualize domains of PSII CC bound to DCPU-lipid monolayers. SNOM imaging has enabled us to confirm that domains observed by AFM were composed of PSII CC. Indeed, the SNOM topography images presented similar domains as those observed by AFM, but in addition, it allowed us to determine that these domains are fluorescent. Electron microscopy of these domains, however, has shown that the bound PSII CC was not crystalline.

INTRODUCTION

Photosystem II (PSII) is a multisubunit complex comprising more than 25 different proteins and photosynthetic pigments, such as chlorophyll (Chl) (Hankamer and Barber, 1997). In higher plants, PSII is located in the thylakoid membrane of chloroplasts, where the first light-driven steps of photosynthesis occur. Upon light absorption, PSII catalyzes electron transfer reactions from water to the electron transporter plastoquinone (Hankamer and Barber, 1997; Hansson and Wydrzynski, 1990; Vermaas, 1993). This photooxidation process is coupled to the evolution of oxygen and is essential to any animal life.

A large number of structural studies of PSII by electron microscopy were conducted to produce three-dimensional models of the complex (Barber and Kühlbrandt, 1999; Hasler et al., 1997; Marr et al., 1996a,b; Nield et al., 2000a,b). A high-resolution structure of PS II has not been determined so far, but two different PSII complex structures have been obtained to a resolution that reveals the secondary structure of the membrane protein (Hankamer et al., 1999; Hasler et al., 1997; Mayanagi et al., 1998; Rhee et al., 1998). There is still substantial research going on to improve the models and determine the structure of PSII at higher resolution (for a review of the advances on PSII structure, see Barber and Kühlbrandt, 1999; Hankamer and Barber, 1997). Until now, electron crystallography has revealed the location of important subunits and photoactive pigment molecules within PSII proteins (Barber and Kühlbrandt, 1999). The development of new methods to obtain high-quality crystals of this protein complex could provide new insights into the structure of PSII.

Hirata and Miyake (1994) have shown that functionalized lipids can be designed to bind the bacterial photosynthetic reaction center onto monolayers at the air-water interface on the basis of the pioneering work by Kornberg's group with soluble proteins (Uzgiris and Kornberg, 1983). Such an approach could thus be used to anchor PSII CC and, eventually, prepare two-dimensional (2D) crystals if proper binding to a lipid monolayer can be achieved.

In this work, we investigated PSII core complex (PSII CC), which is the smallest complex (with molecular mass of 240 kDa) able to evolve molecular oxygen. This subcomplex of PSII contains CP47, CP43, D1, D2, and subunits of cytochrome (cyt) b_{559}, psbI gene product, and the extrinsic 33-kDa protein, as well as all functional cofactors located in those polypeptides that are essential to photosynthesis. Many herbicides have been shown to specifically bind the Q_B site on the D1 protein, by competition with plastoquinone, and could thus be used for PSII CC anchoring onto a lipid support (Petrouleas and Diner, 1987).

Here we present the design and the monolayer characterization of functionalized lipids bearing a dichlorophenyl urea (DCPU) group. Binding of PSII CC to DCPU-lipids

Received for publication 5 December 2000 and in final form 19 April 2001.

Address reprint requests to Dr. Christian Salesse, Département de Chimie-Biologie, Université du Québec à Trois-Rivières, CP 500, Trois-Rivières, Québec G9A 5H7, Canada. Tel.: 819-376-5011; Fax: 819-376-5057; E-mail: christian_salesse@uqtr.uquebec.ca.

0006-3495/01/07/563/09 $2.00

has been investigated in a micellar solution by oxygen evolution measurements as well as by atomic force microscopy (AFM) and scanning near-field optical microscopy (SNOM). Though the resolution of SNOM is limited when compared with AFM, it has the advantage of combining both topography and fluorescence imaging capabilities. By using these techniques, we were able to correlate fluorescence and topography of PSII CC bound to the functionalized DCPU-lipids. Preliminary 2D crystallization trials were performed, and protein close-packing was analyzed by transmission electron microscopy (TEM).

MATERIALS AND METHODS

Purification of PSII CC

PSII CC was extracted from fresh spinach leaves by the method described by Gallant et al. (1998) on the basis of the original method of van Leeuwen et al. (1991). Sample buffer (BTS) used to prepare PSII CC contained 20 mM bis(2-hydroxyethyl) imino-tris (hydroxymethyl) methane (Bis-Tris, Sigma Chemical Co., St. Louis, MO) at pH 6.5, 20 mM $MgCl_2$ (Fisher Scientific Co., Fair Lawn, NJ), 5 mM $CaCl_2$ (Omega Chemical Co., Québec, Canada), 75 mM $MgSO_4$ (Sigma), 400 mM sucrose (ACP Chemicals, Montreal, Canada), and 0.03% (w/v) *n*-dodecyl-β-D-maltoside (DM) (Calbiochem, San Diego, CA). The concentration of PSII CC samples was determined spectroscopically according to the method of De Las Rivas et al. (1995) using the known extinction coefficient for cyt b_{559} (17.5 mM^{-1} cm^{-1}). All manipulations involving PSII CC samples were performed under dim green light.

Synthesis and characterization of DCPU-lipids

Compounds 1–4 were prepared using previously described procedures (Ibanez 1976; Karu et al., 1994; Schenach et al., 1966; Schneider et al., 1994). Compound 5 resulted from the reaction of the tetrahydropyranyl ether of 2-{2-[2-(2-methylamino-ethoxy)-ethoxy]-ethoxy}-ethanol with 3,4-dichlorophenyl isocyanate and subsequent removal of the hydroxyl protective group using pTsOH/methanol. The DCPU-lipids 6 and 7 were synthesized from 3,4-dichlorophenyl isocyanate and the corresponding 1,3-dialkoxy-2-(α-methylamino) acetamido propane. DCPU-lipids 8 and 9 were obtained through oxidation of compound 5 and coupling of the resulting carboxylic acid with the corresponding 1,3-dialkoxy-2-amino propane.

Reactions were monitored by thin-layer chromatography (TLC; Merck precoated plates 0.25 mm, silica gel 60 F_{254}, 0.040–0.060 mm, 230–400-mesh American Society for Testing and Materials (ASTM). Compounds were purified to homogeneity by flash chromatography over silica gel 60 (Merck, 0.040–0.060 mm, 230–400-mesh ASTM). ^{1}H- and ^{13}C-NMR spectra were recorded on Brucker-WP-200-Sy or Brucker-Avance-DPX-300 spectrometers, and chemical shifts δ are in ppm relative to an internal reference (^{1}H: $CHCl_3$ at 7.27 ppm or $CDHCl_2$ at 5.35 ppm; ^{13}C: $CDCl_3$ at 77.0 ppm or CD_2Cl_2 at 53.5 ppm). Infrared (IR) spectra were recorded on Perkin-Elmer-1600-FTIR or Perkin-Elmer-Spectrum2000-FTIR spectrometers, and absorption values are in cm^{-1}. Mass spectra (MS) were recorded on a Finnigan-4600 quadrupole instrument at chemical ionization. Mass data are reported in mass units (*m*/*z*). Abbreviations are as follows: s, singlet; d, doublet; t, triplet; h, heptuplet; q, quintuplet; m, multiplet; b, broad.

For 3-(3,4-dichlorophenyl)-1-(2-{2-[2-(2-hydroxyethoxy)-ethoxy]-ethoxy}-ethyl)-1-methylurea (compound 5), values are as follows: TLC (CH_2Cl_2/CH_3COCH_3 3/1), R_f = 0.15; ^{1}H-NMR ($CDCl_3$, 300 MHz), 8.16 (s, 1 H), 7.56 (dd, J = 1.1, 1.9 Hz, 1 H), 7.30 (dd, J = 1.1, 7.5 Hz, 1 H), 7.29 (dd, J = 1.9, 7.5 Hz, 1 H), 3.76–3.49 (m, 16 H), and 3.01 (s, 3 H); ^{13}C-NMR ($CDCl_3$, 50 MHz), 156.6, 139.9, 132.1, 130.1, 124.7, 120.4, 118.4, 72.4, 70.7, 70.5, 70.3, 70.1 (m), 61.6, 50.2, and 35.1; MS (Cl NH_3), 395 $[M+H]^+$ and 412 $[M+NH_4]^+$; IR (film), 3323, 2875, 1656, 1587, 1523, 1477, 1396, 1302, 1227, 1131, and 1071.

For 2-[3-(3,4-dichlorophenyl)-1-methylureido]-*N*-(2-octadecyloxy-1-octadecyloxymethyl-ethyl) acetamide (compound 6), values are as follows: TLC (CH_2Cl_2/AcOEt 8/2), R_f = 0.35; ^{1}H-NMR ($CDCl_3$, 300 MHz), 7.63 (d, J = 2.6 Hz, 1 H), 7.49 (s, 1 H), 7.34 (d, J = 9.0 Hz, 1 H), 7.24 (dd, J = 2.6, 9.0 Hz, 1 H), 6.33 (d, J = 8.3 Hz, 1 H), 4.30–4.18 (m, 1 H), 3.97 (s, 2 H), 3.56 (dd, J = 4.5, 9.4 Hz, 2 H), 3.47 (dd, J = 6.0, 9.4 Hz, 2 H), 3.44 (t, J = 6.8 Hz, 4 H), 3.10 (s, 3 H), 1.61–1.48 (m, 4 H), 1.39–1.20 (m, 60 H), and 0.95–0.85 (m, 6 H); ^{13}C-NMR ($CDCl_3$, 75 MHz), 169.3, 156.2, 138.9, 132.6, 130.4, 126.2, 121.5, 119.2, 71.6, 68.6, 53.6, 49.1, 36.3, 32.1, 29.9, 29.8, 29.7, 29.6, 29.5 (m), 26.3, 22.9, and 14.3; MS (CI NH_3), 855 $[M+H]^+$; IR (film), 3285, 2917, 2850, 1646, 1586, 1535, 1470, 1370, 1286, 1231, 1124, and 1095.

For 2-[3-(3,4-dichlorophenyl)-1-methylureido]-*N*-(2-octadec-8-enyloxy-1-octadec-8-enyloxymethyl-ethyl) acetamide (compound 7), values are as follows: TLC (CH_2Cl_2/AcOEt 8/2), R_f = 0.30; ^{1}H-NMR ($CDCl_3$, 300 MHz), 7.63 (d, J = 2.2 Hz, 1 H), 7.57 (s, 1 H), 7.32 (d, J = 8.6 Hz, 1 H), 7.24 (dd, J = 2.2, 8.6 Hz, 1 H), 6.38 (d, J = 8.3 Hz, 1 H), 5.44–5.27 (m, 4 H), 4.30–4.18 (m, 1 H), 3.96 (s, 2 H), 3.55 (dd, J = 4.5, 9.4 Hz, 2 H), 3.46 (dd, J = 6.0, 9.4 Hz, 2 H), 3.43 (t, J = 6.8 Hz, 4 H), 3.09 (s, 3 H); 2.12–1.92 (m, 8 H), 1.62–1.47 (m, 4 H), 1.42–1.18 (m, 44 H), and 0.96–0.82 (m, 6 H); ^{13}C-NMR ($CDCl_3$, 75 MHz), 169.3, 156.0, 138.9, 132.6, 130.4, 130.1, 129.9, 126.2, 121.5, 119.2, 71.7, 68.9, 53.6, 49.0, 36.3, 32.1, 29.9 (m), 29.8, 29.7 (m), 29.6 (m), 29.5 (m), 27.3 (m), 26.3, 22.8, and 14.3; MS (CI NH_3), 851 $[M+H]^+$; IR (film), 3300, 2926, 2854, 1799, 1762, 1652, 1589, 1521, 1476, 1393, 1288, 1229, 1125, and 816.

For 2-[2-(2-{2-[3-(3,4-dichlorophenyl)-1-methylureido]-ethoxy}-ethoxy)-ethoxy]-*N*-(2-octadecyloxy-1-octadecyloxymethyl-ethyl) acetamide (compound 8), values are as follows: TLC (CH_2Cl_2/AcOEt 1/1), R_f = 0.45; ^{1}H-NMR ($CDCl_3$, 300 MHz), 8.16 (s, 1 H), 7.52 (dd, J = 2.2, 8.7 Hz, 1 H), 7.31 (dd, J = 2.2, 8.7 Hz, 1 H), 7.29 (dd, J = 2.2, 8.7 Hz, 1 H), 6.91 (d, J = 8.7 Hz, 1 H), 4.29–4.18 (m, 1 H), 4.09 (s, 2 H), 3.76–3.65 (m, 10 H), 3.57–3.39 (m, 10 H), 3.01 (s, 3 H); 160–1.48 (m, 4 H), 1.38–1.21 (m, 60 H), and 0.92–0.84 (m, 6 H); ^{13}C-NMR ($CDCl_3$, 50 MHz), 169.5, 156.6, 140.1, 132.3, 130.3, 124.9, 120.4, 118.4, 71.5, 71.0, 70.9, 70.7, 70.6 (m), 68.9, 50.4, 48.0, 35.4, 32.1, 29.9–29.5 (m), 26.2, 22.8, and 14.3; MS (CI NH_3), 988 $[M+H]^+$; IR (film), 3285, 2911, 2843, 1648, 1582, 1535, 1467, 1365, 1230, 1120, and 1092.

For 2-[2-(2-{2-[3-(3,4-dichlorophenyl)-1-methylureido]-ethoxy}-ethoxy)-ethoxy]-*N*-(2-octadec-8-enyloxy-1-octadec-8-enyloxymethyl-ethyl) acetamide (compound 9), values are as follows: TLC (CH_2Cl_2/AcOEt 1/1), R_f = 0.45; ^{1}H-NMR (CD_2Cl_2, 300 MHz), 8.22 (s, 1 H), 7.61 (m, 1 H), 7.32 (m, 1 H), 7.29 (m, 1 H), 6.87 (d, J = 8.6 Hz, 1 H), 5.42–5.32 (m, 4 H), 4.24–4.14 (m, 1 H), 3.97 (s, 2 H), 3.77–3.65 (m, 10 H), 3.56–3.41 (m, 10 H), 3.00 (s, 3 H), 2.19–1.95 (m, 8 H), 1.62–1.50 (m, 4 H), 1.47–1.23 (m, 44 H), and 0.96–0.86 (m, 6 H); ^{13}C-NMR ($CDCl_3$, 75 MHz), 169.2, 156.3, 140.6, 132.1, 130.2, 130.0, 129.9 (m), 124.3, 120.3, 118.4, 71.4, 71.0–70.5 (m), 69.2, 50.4, 48.2, 35.1, 32.1, 29.9–29.5 (m), 27.3 (m), 26.3, 22.8, and 14.0; MS (CI NH_3), 984 $[M+H]^+$; IR (film), 3328, 2926, 2855, 1800, 1679, 1588, 1522, 1477, 1394, 1303, 1230, 1120, and 1031.

Measurement of PS II CC oxygen evolution

Oxygen evolution measurements were performed with a Clark-type electrode cell (Hansatech, Norfolk, UK). The cell contained PSII CC at a Chl concentration of 5 μM and 1 mM 2,5-dichloro-*p*-benzoquinone (DCBQ) (Aldrich, Oakville, Ontario, Canada), a plastoquinone analog that acts as an electron acceptor. The solution was kept at 20°C during experiments. We used a saturating red light centered at 660 nm to induce oxygen evolution. The measured oxygen evolution of PSII CC was 1235 ± 30 μmol of O_2/mg Chl · h, which is similar to other results reported in the literature (Fotinou

et al., 1993; Rogner et al., 1996). For affinity measurements with water-soluble derivatives of 3-(3,4-dichlorophenyl)-1,1-dimethylurea (DCMU), i.e., compounds 1–5 (DCPUs), oxygen evolution was detected for concentrations ranging from 10^{-9} to 10^{-3} M. Affinity of DCPU-lipids 6–9 toward PSII CC has been measured in the same conditions as for the water-soluble compounds, except that DM (4.4% w/v) was used to solubilize the lipids.

Monolayer characterization of the DCPU-lipids

Surface pressure isotherms were measured on a home-made Langmuir trough that has recently been described (Gallant et al., 1998). DCPU-lipids were dissolved in chloroform (Megasolv-HPLC 99.98%, Omega Chemical Co., Lévis, Québec, Canada) and spread over nano-pure water filtered from a four-cartridge system (NANOpure SYBRON, Barnstead, Boston, MA). The specific resistivity and surface tension of ultrapure water was 18×10^6 Ω cm and 72.5 mN/m, respectively. Surface pressure (π) was detected with a Wilhelmy plate system using a filter paper (Albrecht, 1983). Monolayers were compressed at 7 Å^2/molecule min, and each experiment was run in triplicate, the experimental error being smaller than 1 Å^2/molecule.

AFM and SNOM measurements of lipid-bound PSII CC

AFM images of the films were recorded in intermittent contact mode with a commercially available instrument (model Discoverer TMX 2010, TopoMetrix, Sunnyvale, CA). Silicon tips mounted on Topometrix 1660 silicon cantilevers had a resonance frequency of 170 kHz with a force constant of 45 N/m. A 40% amplitude damping was used as feedback parameter and using a scan rate of 1 Hz (lines per second). Trace and retrace images were compared to correct for friction-induced height artifacts.

The SNOM apparatus was a modified commercially available instrument (model Aurora, Topometrix). To allow detection of fluorescence up to 800 nm, the laser diode used for the shear force feedback was replaced by an external laser diode with a wavelength of 980 nm (model C86147E, EG&G, Vaudreuil, Québec, Canada). The photomultiplier tube was replaced by a more sensitive detector with a single-photon avalanche photodiode module (model SPM-CD1718, EG&G). As excitation source, an argon ion laser tuned to 458 nm was used. The laser light was coupled into the SNOM filter probe via a single-mode fiber coupler. Excitation light to the detector was blocked by a holographic laser notch filter (Kaiser Optical Systems, Ann Arbor, MI). Additional IR short-pass filters (CVI SPF-900) were used to block the light from the shear force measurement module. Fluorescence was measured in transmission mode by collecting the emitted light with an objective (60×/NA 0.70, Nikon, Melville, NY). Home-made SNOM probes were used. The experimental setup is described in more detail elsewhere (Vanoppen et al., 1998).

Custom-designed Teflon wells used for the protein-binding experiments on lipid films were 18 mm in diameter and 4 mm deep. PSII CC in BTS buffer (1.2 ml, 250 μg/ml) was first deposited into the wells. Then, a DCPU-lipid solution (24 μl, 0.5 mg/ml) was spread on the surface of this protein solution. After a 2-h incubation, silanized glass plates (18 mm × 18 mm) were horizontally deposited on top of the wells and withdrawn after 1–2 s of adsorption. The plates were rinsed with nano-pure water and stored in a dessicator at 4°C in darkness until use.

Crystallization trials and electron microscopy

Two-dimensional crystallization trials of PSII CC were performed by spreading 0.5 μl of DCPU-lipids at the surface of a solution containing 36 μl of PSII CC (50–500 mg/ml in BTS buffer) in Teflon wells (4 mm in diameter and 4 mm deep). DCPU-lipids (0.1–1.0 mg/ml in chloroform) were assayed either pure or as mixtures (1–10 mol %, 0.1–1.0 mg/ml) with phospholipids. Saturated DCPU-lipids 6 and 8 were mixed with 1,2-dipalmitoyl-*sn*-glycero-phosphatidylcholine (DPPC) whereas unsaturated DCPU-lipids 7 and 9 were mixed with 1,2-dioleoyl-*sn*-glycero-phosphatidylcholine (DOPC). Incubation with PSII CC was run in a closed humid chamber to prevent buffer evaporation. A carbon-coated grid was then placed on the top of the well, withdrawn, and negatively stained with two drops of 1% uranyl acetate. Crystallization trials involving detergent removal by Bio-Beads SM2 (Bio-Rad, Hercules, CA) were performed as described by Levy et al. (1999) with slight modifications. The home-made Teflon wells were 4 mm in diameter and 5 mm deep with a hole on the side for the injection of the Bio-Beads and the lipid-protein solution at the bottom of the wells (Levy et al., 1999). A DCPU-lipid solution (0.5 μl, 0.1 mg/ml in chloroform) was spread at the surface of a droplet of the BTS buffer (without PSII CC) in the wells and incubated for 15 min. Six microliters of lipid-PSII CC solution (0.1 mg/ml PSII CC mixed with 0.1 mg/ml monogalactosyl diglyceride (MGDG) (Matreya, Pleasant Gap, PA) containing 10 mM DM and 0.02% (w/v) sodium azide) in BTS was then injected into the wells. After 1 h of incubation under gentle stirring, 5 mg of Bio-Beads were injected into the wells. After 2 h of incubation, an additional 5 mg Bio-Beads portion was added. After a total incubation time of 4 h, films were transferred onto carbon-coated grids and negatively stained with 1% (w/v) uranyl acetate. Micrographs were taken with a Philips EM-208s transmission electron microscope operating at 80 kV.

RESULTS AND DISCUSSION

PSII CC oxygen evolution inhibition by DCMU analogs

Many herbicides compete with the natural electron transporter plastoquinone for the binding to the Q_B site of PSII CC. Because they do not act as electron acceptors, they competitively block the light-induced electron transfer from water to the Q_B site, thereby inhibiting oxygen evolution. Ultimately, the whole photosynthesis process is interrupted. A considerable amount of data is available on PSII-specific herbicides, but still, the action mode is not understood at the molecular level for most of these compounds due to the lack of a high-resolution structure of PSII.

Among herbicides binding the Q_B site of PSII CC, different classes of compounds can be found including phloroglucinols, cyanoacrylates, triazines, and phenylurea (Oettmeier, 1992). Due to the possible degradation of the D1 polypeptide of PSII CC by phloroglucinols (Kirilovsky et al., 1994; Nakajima et al., 1995), to the water sensitivity of the ester function in acrylates, and to the sharp dependence of affinity for the Q_B site on steric factors in triazines, we considered phenylureas as the best candidates for chemical modifications, allowing us to preserve binding to the Q_B site of PSII CC (for a review see Bowyer et al., 1991). Consequently, we designed ligands able to bind the Q_B site of PSII CC based on the DCMU structure. The modification of DCMU analogs through the introduction of a linker to be further connected to a lipid will presumably modify its affinity for the Q_B site of PSII CC. To check that, four different structural analogs of DCMU (Fig. 1) were synthesized and their affinity for PSII characterized by measurements of oxygen evolution in the presence of a competitive electron acceptor of similar structure, DCBQ. The I_{50} values

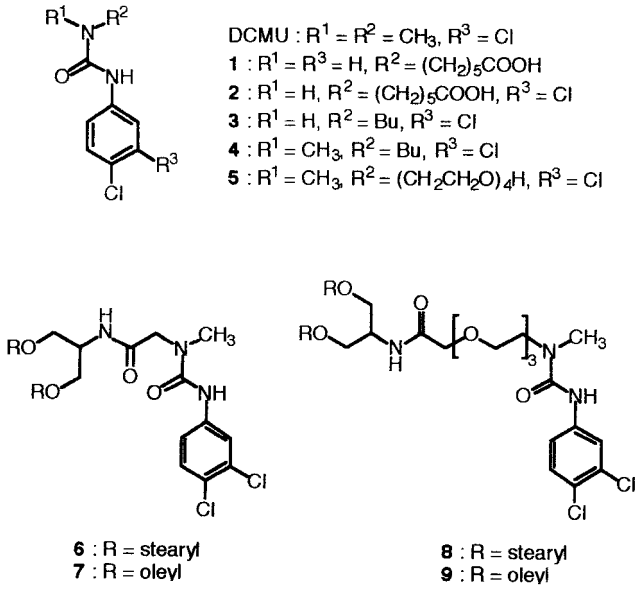

FIGURE 1 Structure of DCMU analogs and functionalized DCPU-lipids.

for the DCMU analogs, which correspond to the concentration of a compound needed to reduce the initial oxygen evolution of PSII CC by 50%, are presented in Table 1. Our results show that compound 4 exhibits the highest affinity for the Q_B site of PSII CC ($I_{50} = 1.2 \times 10^{-7}$ M), even higher than DCMU ($I_{50} = 9.0 \times 10^{-7}$ M). The differences in affinity between compound 1 ($I_{50} > 10^{-3}$) and compound 2 ($I_{50} = 1.2 \times 10^{-4}$) indicates that a second chlorine atom on the aromatic ring is critical for binding to the Q_B site, which is consistent with the work of Satoh et al. (1995). Finally, Table 1 clearly indicates that the polarity of the nitrogen substituents (Fig. 1, R^2) has a strong influence on affinity for the Q_B site of PSII CC. The more hydrophilic is the spacer, the more the affinity for the Q_B site of PSII CC of the analog will be reduced (caproic acid (2) < hydroxypolyether (5) < butyl (4)). Compound 4 has thus been used for the synthesis of DCPU-lipids.

Monolayer characterization of DCPU-lipids

Surface pressure versus molecular area (π-A) isotherms of the four DCPU-lipids are presented in Fig. 2. Both saturated

TABLE 1 I_{50} values calculated from oxygen evolution measurements of DCMU and its DCPU analogs in the presence of 1 mM DCBQ

Compound	I_{50} (M)
DCMU	9.0×10^{-7}
1	$>10^{-3}$
2	1.2×10^{-4}
3	2.0×10^{-6}
4	1.2×10^{-7}
5	5.0×10^{-5}

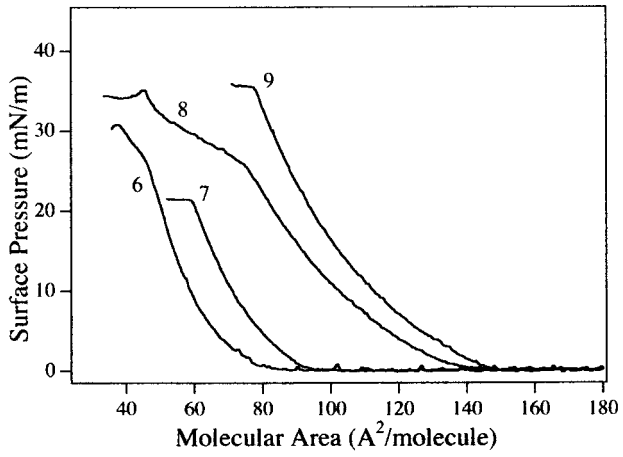

FIGURE 2 Surface pressure-area isotherms of DCPU-lipids 6–9 on pure water at 20.0 ± 0.5°C.

DCPU-lipids 6 and 8 show a phase transition from the liquid-expanded (LE) to liquid-condensed (LC) state at ~25 mN/m whereas the two unsaturated DCPU-lipids 7 and 9 show a LE state throughout the isotherm. Collapse of DCPU-lipids 6, 7, 8, and 9 occurs at ~30, 20, 36, and 36 mN/m, respectively. Molecular area before the onset of the collapse pressure of lipids 6, 7, 8, and 9 occurs at 40, 60, 42, and 80 Å^2/molecule, respectively. DCPU-lipids 8 and 9, bearing a long ethylene oxide spacer, obviously occupy a much larger area than DCPU-lipids 6 and 7, which do not contain such a spacer. Indeed, the molecular area of 80 and 95 Å^2/molecule at the lift-off pressure of DCPU-lipids 6 and 7, respectively, is much smaller than in the case of DCPU-lipids 8 and 9 (145 and 150 Å^2/molecule, respectively).

Films prepared with DCPU-lipids 8 and 9 collapse at higher surface pressures, and their surface pressure is much more stable over time than DCPU-lipids 6 and 7 (data not shown). Obviously, the hydrophilic ethylene oxide spacer provides more stability to these lipids. The increased hydrophilicity of the polar headgroup is likely providing DCPU-lipids 8 and 9 with a more adequate hydrophilic/hydrophobic balance. The ability of these lipids to form stable monolayers is of great importance for protein anchoring and two-dimensional crystallization purposes, because monolayers of functionalized lipids are incubated over a few hours at high surface pressure. Thus, DCPU-lipids 8 and 9 were chosen for binding and anchoring of PSII CC.

Evidence for the binding of DCPU-lipids to PSII CC by oxygen evolution measurements

Oxygen evolution experiments with DCPU-lipids were performed to demonstrate the specific binding between these lipids and the Q_B site of PSII CC. These affinity measurements were performed with the two long-spacer DCPU-lipids 8 and 9. Fig. 3 shows that both DCPU-lipids 8 and 9

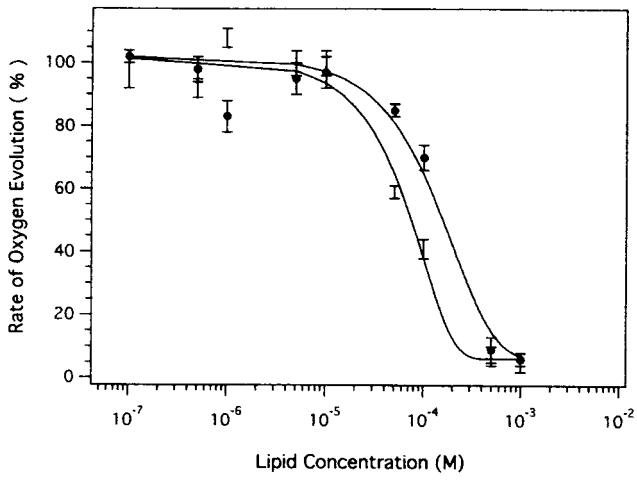

FIGURE 3 Effect of DCPU-lipids 8 (●) and 9 (○) on the oxygen evolution of PSII CC determined in the presence of 1 mM DCBQ and 4.4% w/v DM.

are able to compete with DCBQ to bind the Q_B site of PSII CC and inhibit electron transport, thus reducing oxygen evolution. The I_{50} values calculated from oxygen evolution are 2×10^{-4} M and 7×10^{-5} M for DCPU-lipids 8 and 9, respectively. The I_{50} value obtained for DCPU-lipid 9 is very close to the one obtained for compound 5 (Table 1), indicating in this case that the lipid moiety does not alter the ligand-protein recognition process. On the other hand, with DCPU-lipid 8, the I_{50} value increased by one order of magnitude, thus showing a reduced affinity for PSII CC compared with compound 5. Nonetheless, the observation of a reduction of oxygen evolution of PSII CC by DCPU-lipids 8 and 9 suggests that these lipids bind specifically to the Q_B site of PSII CC, thereby replacing the electron acceptor DCBQ. This result suggests that these lipids can be used for anchoring PSII CC and, eventually, for two-dimensional crystallization experiments.

AFM and SNOM imaging of PSII CC bound to DCPU-lipid films

Intermittent contact mode AFM is a well established method to obtain high-resolution topography images of biological material (Dinte et al., 1996; Morita et al., 1996; Radmacher et al., 1995). SNOM is particularly useful for the present study as it combines the ability of obtaining topography and fluorescence images of the sample, because PSII CC is highly fluorescent. The presence of PSII CC can thus be directly assayed by the observation of the fluorescence distribution in the sample. AFM and SNOM imaging were used to show that the binding of PSII CC to DCPU-lipids in micellar solutions (Fig. 3) is also occurring with monolayers of DCPU-lipids. DCPU-lipids spread over a solution of PSII CC were transferred onto a solid substrate after 2 h of incubation and then observed by AFM and SNOM.

Fig. 4 shows a typical AFM image of PSII CC adsorbed onto a film of DCPU-lipid 8 where numerous large domains can be observed. These domains appear to be composed of small globular shapes, presumably made of PSII CC. From various line scans calculated from the AFM topography images, the thickness of these domains vary from 20 to 30 nm on average (Fig. 5), but can be as large as 40–60 nm (Fig. 4). The uniformity between domains, which corresponds to the darker areas on the AFM images, suggests that a rather homogeneous lipid film covers the glass substrate. The same type of structure was also observed when using pure DCPU-lipid 9. Moreover, when PSII CC is adsorbed onto a film of DPPC instead of DCPU-lipids 8 or 9, films are homogeneous, similar to the dark areas observed in Fig. 4, and do not show any structure thicker than 2 nm (result not shown). This result suggests that the domains observed in the presence of DCPU-lipid layers consist of PSII CC and that DCPU-lipids are necessary for the binding of PSII CC. Previously published results of AFM measurements with transferred PSII membranes by the Langmuir-Blodgett method showed a similar distribution and globular appearance of the PSII particles (Shao et al., 1997). However, the authors used the intermittent-mode AFM with forces (5 nN) that are known to damage soft samples (usually larger than 2 nN) (Grandbois et al., 1998; Muller et al., 2000; Yip et al., 1998). Their observation of a cavity in the central region of the PSII particles may thus be induced by the use of an excessive force.

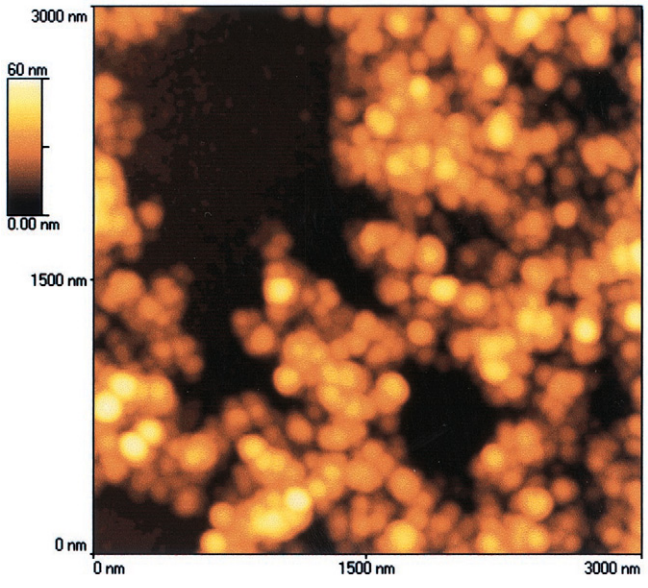

FIGURE 4 AFM topography image in intermittent contact mode of PSII CC bound to a DCPU-lipid 8 layer. Pure DCPU-lipids in chloroform are spread onto a droplet of a PSII CC solution. After a 2-h incubation, lipid-protein complexes are then transferred onto a silanized glass plate. Samples were dried and measured in air.

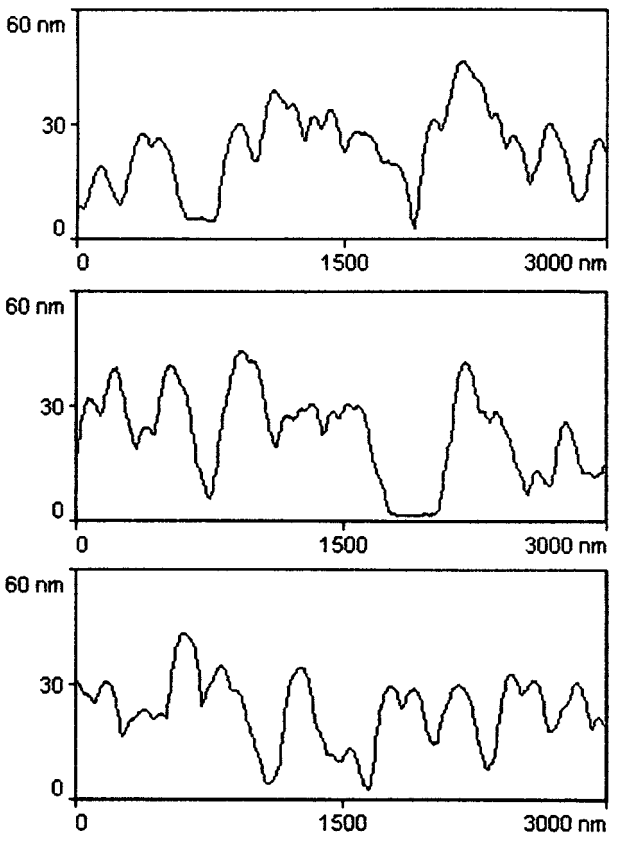

FIGURE 5 Various representative *x-z* line scans calculated from the AFM images. The smaller globular domains can be recognized as peaks of ~150–375 nm wide and have a average thickness of 20–30 nm.

According to previously published models of PSII, the dimensions of a PSII CC dimer are ~15 × 20 nm in the membrane plane and 11 nm perpendicular to this plane (Hankamer and Barber 1997; Hankamer et al., 1999). Another model of the PSII core dimer from thermophilic cyanobacterium *Synechococcus elongatus* was recently presented by Nield et al. (2000b). They estimated the overall dimensions of the PSII core dimer to be 15 × 22 nm in the plane of the membrane and 9.5 nm in the axis perpendicular to the membrane. Despite the fact that the subunit composition of the cyanobacterium core dimer differs from that of the spinach PSII CC in our experiments, their structure is remarkably similar (Boekema et al., 1995). There is a general consensus emerging from numerous structural studies in favor of the dimerization state of PSII (Hankamer et al., 1999; Kruse et al., 2000; Lyon, 1998; Nield et al., 2000a). Such an organization would lead to a minimum thickness of ~20 nm, which is comparable to the thickness of the domains observed by AFM and SNOM. A possible molecular organization of PSII CC that would explain the dimensions of the domains observed by AFM would thus be that dimers of PSII CC are bound to DCPU-lipids at the Q_B site of PSII CC. The 20–30-nm thickness values measured by AFM and SNOM would thus correspond to the dimensions of PSII CC organized as a dimer as postulated in Fig. 6. On the other hand, from the AFM image one can see that the dimensions of the globular-shaped domains in the plane of the monolayer are variable in size and do not present any ordered, crystalline pattern.

The same type of protein domains can also be distinguished in the SNOM topography images as shown in Fig. 7. The smaller globular domains of PSII CC observed by AFM (Fig. 4) are not apparent in the SNOM topography and fluorescence images. This can be explained by the best achievable lower lateral resolution obtained by SNOM (~20–30 nm) compared with AFM (~1–5 nm) because of the size of the probing tip, both in ideal circumstances (Moller et al., 1999). On the other hand, the film thickness obtained by SNOM is in good agreement with the one measured by AFM (compare Figs. 5 and 7 *A*).

PSII CC shows strong excitation and emission bands centered at 440 and 680 nm, respectively (Haag et al., 1990). The images shown in Fig. 7 *B* were generated by exciting the film with a laser at 458 nm and collecting the fluorescence with a 515-nm long-pass filter. The fluorescence observed in this image should thus unambiguously originate from PSII CC (Haag et al., 1990). It can be seen that globular domains of 20–30-nm thickness present a high fluorescence compared with the background, where fluorescence intensity values are approximately as high as the noise level. SNOM images demonstrated a clear correlation between topography and fluorescence, showing that those transferred domains emit fluorescence above 515 nm and can thus be assigned to the presence of bound PSII CC.

In a previous work, Hirata and Miyake (1994) studied the binding of quinone-depleted bacterial photosynthetic reaction center (RC) to quinonylphospholipids in the scope to use this system for the preparation of new molecular devices. The binding of the RC to the lipid monolayer was first demonstrated by the increase in molecular area of the film. Nonspecific interaction between the protein and the lipid interface could also contribute to this increase in molecular

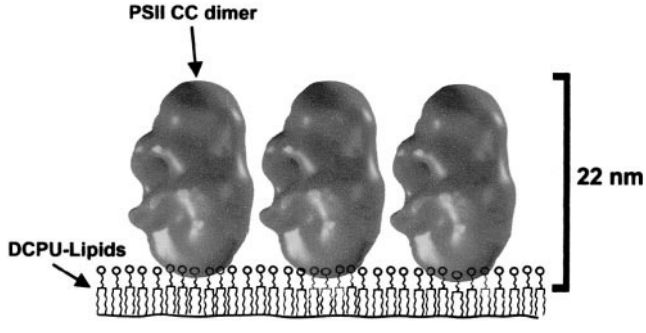

FIGURE 6 Proposed model for the binding of PSII CC to the DCPU-lipid monolayer. The model of PSII CC comes from the data published by Nield et al. (2000a)

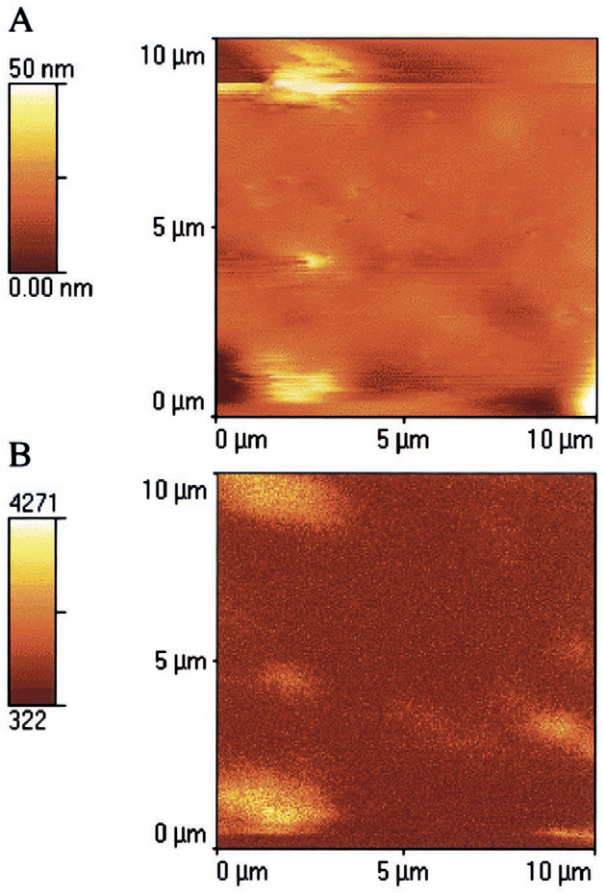

FIGURE 7 SNOM images of a film of PSII CC bound to a layer of DCPU-lipid 8. (*A*) Topography mode; (*B*) Fluorescence mode using a 458-nm excitation wavelength and a 515-nm long-pass filter. The color scale bar to the left is in counts per second.

area. Thus, this measure is not sufficient to demonstrate specific binding of the RC to the functionalized lipids. In the case of the work of Hirata and Miyake (1994) with photosynthetic RC, the photobleaching of the film indicates the binding of the quinone moiety, as it is incorporated into its binding site of RC. In the present work, we showed the presence of PSII CC on the DCPU-lipid film by AFM as well as by SNOM topography imaging. The specific binding of PSII CC to the DCPU-lipids is directly visualized with the SNOM images. Indeed, the absence of PSII CC when DPPC was used instead of DCPU-lipids suggests that a specific binding is taking place between PSII CC and DCPU-lipids.

Since we have demonstrated that specifically bound PSII CC to DCPU-lipid films can be transferred onto solid hydrophobic substrates, two-dimensional crystallization trials were then performed under a large number of experimental conditions. Parameters that were varied included protein, salt and detergent concentration of the solubilization buffer, temperature, incubation time, concentration of the DCPU-lipids, and use of different natural lipid matrices for the DCPU-lipids. However, no crystalline structure could be observed by electron microscopy. This could be due to the presence of the detergent used to solubilize PSII CC, which, in turn, can disrupt the lipid monolayer. Nonetheless, Levy et al. (1999) recently succeeded in preparing 2D crystals of two large membrane proteins with functionalized lipids using a new approach where the detergent is removed by adsorption on polystyrene beads. The use of a detergent to solubilize PSII CC is necessary to prevent protein aggregation and possible denaturation in solution. On the other hand, the presence of a detergent in the crystallization trials may disrupt the functionalized DCPU-lipid film. The method of Levy et al. (1999) thus provides a way to gradually adsorb the detergent present in solution onto polystyrene beads that are present in the wells where PSII CC was deposited. Crystallization trials using this method did not yield PSII CC crystals but has enabled us to obtain large domains of close-packed protein (Fig. 8). Preliminary results obtained by electron microscopy demonstrate promising avenues for the crystallization of PSII CC with DCPU-lipids, and additional experimental parameters must be investigated to produce 2D crystals. Systematic crystallization trials are now being conducted.

CONCLUSION

In the work presented here, we describe functionalized lipids bearing a DCPU moiety in their polar headgroup, which is a structural analog of DCMU, a well known herbicide that binds PSII CC. These lipids were designed for PSII CC immobilization onto a lipid layer and, eventually, for 2D crystallization. We have characterized the surface pressure isotherm of these lipids in monolayers at the air-water interface. The binding of these DCPU-lipids to PSII

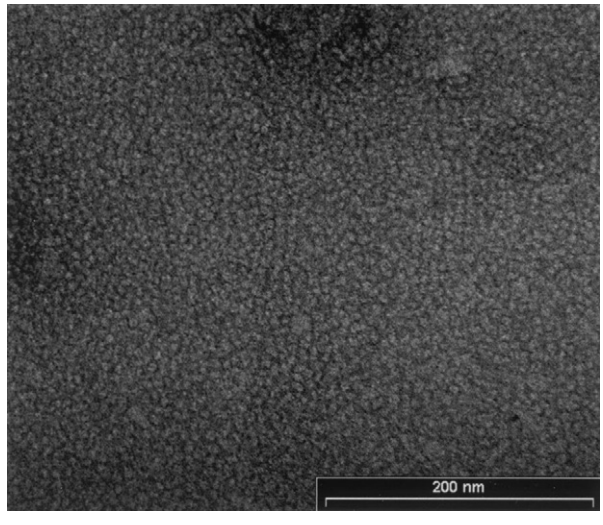

FIGURE 8 Electron micrograph of typical negatively stained 2D close-packing of PSII CC obtained during crystallization trials.

CC was demonstrated by the reduction of the oxygen evolution of PSII CC in micellar solutions as well as by AFM and SNOM imaging. The use of AFM in combination with SNOM fluorescence imaging provides a unique way of studying the specific binding of PSII CC to the lipid monolayer. The 2D crystallization of PSII CC using functionalized DCPU-lipids and analysis of the 2D crystals by electron crystallography could provide a way to a high-resolution 3D model of PSII CC.

We are indebted to the Natural Sciences and Engineering Research Council of Canada and the Fonds FCAR for financial support. C. Salesse is a Chercheur Boursier Senior from the Fonds de la Recherche en Santé du Québec.

REFERENCES

Albrecht, O. 1983. The construction of a microprocessor–controlled film balance for precision measurement of isotherms and isobars. *Thin Solid Films.* 99:227–231.

Barber, J., and W. Kühlbrandt. 1999. Photosystem II. *Curr. Opin. Struct. Biol.* 9:469–475.

Boekema, E. J., B. Hankamer, D. Bald, J. Kruip, J. Nield, A. F. Boonstra, J. Barber, and M. Rogner. 1995. Supramolecular structure of the photosystem II complex from green plants and cyanobacteria. *Proc. Natl. Acad. Sci. U.S.A.* 92:175–179.

Bowyer, J. R., P. Camilleri, and W. F. J. Vermaas. 1991. Photosystem II and its interaction with herbicides. *In* Herbicides, Topics in Photosynthesis. N. R. Baker, M. P. Percival, editors. Elsevier, Amsterdam. 27–85.

De Las Rivas, J., J. Klein, and J. Barber. 1995. pH sensitivity of the redox state of cytochrome b559 may regulate its function as a protectant against donor and acceptor side photoinhibition. *Photosynth. Res.* 46: 193–202.

Dinte, B. P., G. S. Watson, J. F. Dobson, and S. Myhra. 1996. Artefacts in non-contact mode force microscopy: the role of adsorbed moisture. *Ultramicroscopy.* 63:115–125.

Fotinou, C., M. Kokkinidis, W. Haase, H. Michel, and D. Ghanotakis. 1993. Characterization of a photosystem II core and its three-dimensional crystals. *Photosynth. Res.* 37:41–48.

Gallant, J., B. Desbat, D. Vaknin, and C. Salesse. 1998. Polarization-modulated infrared spectroscopy and x-ray reflectivity of photosystem II core complex at the gas-water interface. *Biophys. J.* 75:2888–2899.

Grandbois, M., H. Clausen-Schaumann, and H. Gaub. 1998. Atomic force microscope imaging of phospholipid bilayer degradation by phospholipase A2. *Biophys. J.* 74:2398–23404.

Haag, E., K. D. Irrgang, E. J. Boekema, and G. Renger. 1990. Functional and structural analysis of photosystem II core complexes from spinach with high oxygen evolution capacity. *Eur. J. Biochem.* 189:47–53.

Hankamer, B., and J. Barber. 1997. Structure and membrane organization of photosystem II in green plants. *Annu. Rev. Plant Physiol. Plant Mol. Biol.* 48:641–671.

Hankamer, B., E. P. Morris, and J. Barber. 1999. Revealing the structure of the oxygen-evolving core dimer of photosystem II by cryoelectron crystallography. *Nat. Struct. Biol.* 6:560–564.

Hansson, O., and T. Wydrzynski. 1990. Current perceptions of photosystem II. *Photosynth. Res.* 23:131–162.

Hasler, L., D. Ghanotakis, B. Fedtke, A. Spyridaki, M. Miller, S. A. Müller, A. Engel and G. Tsiotis. 1997. Structural analysis of photosystem II: comparative study of cyanobacterial and higher plant photosystem II complexes. *J. Struct. Biol.* 119:273–283.

Hirata, Y., and J. Miyake. 1994. Molecular construction of a photosynthetic reaction center at the interface by its affinity with quinonylphospholipid. *Thin Solid Films.* 244:865–868.

Ibanez, P. G. 1976. Substituted Ureas. Patent Spain, No ES419150, 5 p.

Karu, A. E., D. J. S. Schmidt, S. J. Richman, C. Cooper, D. Tran and J. Hsu. 1994. Validation of a monoclonal immunoassay for diuron in groundwater. *J. Agric. Food Chem.* 42:310–315.

Kirilovsky, D., A. W. Rutherford, and A. L. Etienne. 1994. Influence of DCMU and ferricyanide on photodamage in photosystem II. *Biochemistry.* 33:3087–3095.

Kruse, O., B. Hankamer, C. Konczak, C. Gerle, E. Morris, A. Radunz, G. H. Schmid, and J. Barber. 2000. Phosphatidylglycerol is involved in the dimerization of photosystem II. *J. Biol. Chem.* 275:6509–6514.

Levy, D., G. Mosser, O. Lambert, G. S. Moeck, D. Bald, and J. L. Rigaud. 1999. Two-dimensional crystallization on lipid layer: a successful approach for membrane proteins. *J. Struct. Biol.* 127:44–52.

Lyon, M. K. 1998. Multiple crystal types reveal photosystem II to be a dimer. *Biochim. Biophys. Acta.* 1364:403–419.

Marr, K. M., D. N. Mastronarde, and M. K. Lyon. 1996a. Two-dimensional crystals of photosystem II: biochemical characterization, cryoelectron microscopy and localization of the D1 and cytochrome b559 polypeptides. *J. Cell Biol.* 132:823–833.

Marr, K. M., R. L. McFeeters, and M. K. Lyon. 1996b. Isolation and structural analysis of two-dimensional crystals of photosystem II from *Hordeum vulgare viridis* zb63. *J. Struct. Biol.* 117:86–98.

Mayanagi, K., T. Ishikawa, C. Toyoshima, Y. Inoue, and K. Nakazato. 1998. Three-dimensional electron microscopy of the photosystem II core complex. *J. Struct. Biol.* 123:211–224.

Moller, C., M. Allen, V. Elings, A. Engel, and D. J. Muller. 1999. Tapping-mode atomic force microscopy produces faithful high-resolution images of protein surfaces. *Biophys. J.* 77:1150–1158.

Morita, S., S. Fujisawa, E. Kishi, M. Ohta, H. Ueyama, and Y. Sugawara. 1996. Contact and non-contact mode imaging by atomic force microscopy. *Thin Solid Films.* 273:138–142.

Muller, D. J., J. B. Heymann, F. Oesterhelt, C. Moller, H. Gaub, G. Buldt, and A. Engel. 2000. Atomic force microscopy of native purple membrane. *Biochim. Biophys. Acta.* 1460:27–38.

Nakajima, Y., S. Yoshida, Y. Inoue, K. Yoneyama, and T. Ono. 1995. Selective and specific degradation of the D1 protein induced by binding of a novel photosystem II inhibitor to the QB site. *Biochim. Biophys. Acta.* 1230:38–44.

Nield, J., O. Kruse, J. Ruprecht, P. da Fonseca, C. Buchel, and J. Barber. 2000a. Three-dimensional structure of *Chlamydomonas reinhardtii* and *Synechococcus elongatus* photosystem II complexes allows for comparison of their oxygen-evolving complex organization. *J. Biol. Chem.* 275:27940–27946.

Nield, J., E. V. Orlova, E. P. Morris, B. Gowen, M. van Heel, and J. Barber. 2000b. 3D map of the plant photosystem II supercomplex obtained by cryoelectron microscopy and single particle analysis. *Nat. Struct. Biol.* 7:44–47.

Oettmeier, W. 1992. Herbicides of photosystem II. *In* The Photosystems: Structure, Function and Molecular Biology. J. Barber, editor. Elsevier, Amsterdam. 349–408.

Petrouleas, V., and B. A. Diner. 1987. Q400, the non-heme iron of photosystem II iron-quinone complex. A spectroscopic probe of quinone and inhibitor binding to the reaction center. *Biochim. Biophys. Acta.* 893:126–131.

Radmacher, M., M. Fritz, and P. K. Hansma. 1995. Imaging soft samples with the atomic force microscope: gelatin in water and propanol. *Biophys. J.* 69:264–270.

Rhee, K. H., E. P. Morris, J. Barber, and W. Kühlbrandt. 1998. Three-dimensional structure of the plant photosystem II reaction centre at 8 Å resolution. *Nature.* 396:283–286.

Rogner, M., E. J. Boekema, and J. Barber. 1996. How does photosystem 2 split water? The structural basis of efficient energy conversion. *Trends Biochem. Sci.* 21:44–49.

Satoh, K., M. Oh-hashi, Y. Kashino, and H. Koike. 1995. Mechanism of electron flow through the QB site in photosystem II. I. Kinetics of the reduction of electron acceptors at the QB and plastoquinone sites in photosystem II particles from the *Cyanobacterium synechococcus vulcanus*. *Plant Cell Physiol.* 36:597–605.

Schenach, T. A., J. J. Brown, A. J. Wysocki, and F. Yackovich. 1966. The bacteriostatic effectiveness of 1-alkyl-3-3,4-dichlorophenyl) ureas. *J. Med. Chem.* 9:426–428.

Schneider, P., M. H. Goodrow, S. J. Gee, and B. D. Hammock. 1994. A highly sensitive rapid ELISA for the arylurea herbicides diuron, monuron, and linuron. *J. Agric. Food Chem.* 42:413–422.

Shao, L., N. J. Tao, and R. M. Leblanc. 1997. Probing the microelastic properties of nanobiological particles with tapping mode atomic force microscopy. *Chem. Phys. Lett.* 273:37–41.

Uzgiris, E. E., and R. D. Kornberg. 1983. Two-dimensional crystallization technique for imaging macromolecules, with application to antigen-antibody-complement complexes. *Nature.* 301:125–129.

van Leeuwen, P. J., M. C. Nieven, E. J. van de Meent, J. P. Dekker, and H. J. van Gorkom. 1991. Rapid and simple isolation of pure photosystem core and reaction particles from spinach. *Photosynth. Res.* 28:149–154.

Vanoppen, P., J. Hofkens, K. Jeuris, H. Faes, J. Kerimo, P. F. Barbara, A. E. Rowan, R. J. M. Nolte, and F. C. De Schryver. 1998. Applied Fluorescence in Chemistry, Biology and Medicine. W. Rettig, B. Strehmel, S. Schrader, H. Seifert, editors. Springer-Verlag, New York.

Vermaas, W. F. J. 1993. Molecular-biological Approaches to analyze photosystem II structure and function. *Annu. Rev. Plant Physiol. Plant Mol. Biol.* 44:457–481.

Yip, C. M., C. C. Yip, and M. D. Ward. 1998. Direct force measurements of insulin monomer-monomer interactions. *Biochemistry.* 37: 5439–5449.